Optical emission diagnostics with electric probe measurements of inductively coupled Ar/O2/Ar-O2 plasmas

T. H. Chung, Hae Ra Kang, and Min Keun Bae

Citation: Phys. Plasmas 19, 113502 (2012); doi: 10.1063/1.4765357
View online: http://dx.doi.org/10.1063/1.4765357
View Table of Contents: http://pop.aip.org/resource/1/PHPAEN/v19/i11
Published by the American Institute of Physics.

Optical emission diagnostics with electric probe measurements of inductively coupled Ar/O_2/Ar-O_2 plasmas

T. H. Chung,[a] Hae Ra Kang, and Min Keun Bae
Department of Physics, Dong-A University, Busan 604-714, Korea

(Received 26 June 2012; accepted 18 October 2012; published online 6 November 2012)

Physical properties of low-pressure inductively coupled argon, oxygen, and Ar-O_2 mixture plasmas are investigated using optical emission spectroscopy (OES) combined with an rf-compensated Langmuir probe measurement. In each gas discharge, the electron density and the electron temperature were obtained by using the probe. The electron temperature was also obtained by OES models and compared with that measured by the probe. The electron temperature was observed to decrease with increasing power and pressure and also observed to decrease with increasing Ar content. Argon metastable densities were calculated based on an optical transition model. In Ar-O_2 discharges, the dissociation fraction of O_2 molecules was estimated using optical emission actinometry. The dissociation fraction was observed to increase with increasing power and Ar content. © *2012 American Institute of Physics*.
[http://dx.doi.org/10.1063/1.4765357]

I. INTRODUCTION

In plasma processing, molecular and mixture gases are used in order to achieve the desired selectivity and to improve the etch rate. Oxygen discharges are widely used for industrial-materials processing, such as dry etching of a photoresist, synthesis of metal oxide, functionalization of polymers, deposition of oxide films, and ashing of samples.[1,2] Oxygen with a mixture of rare gases is usually used as the primary gas for oxidization, formation of passivation layer, or other plasma technologies applied to the production of integrated circuits.

From the viewpoints of both industry and physics, experimental and theoretical investigations of O_2 and of O_2-rare gas mixtures are necessary. The etching of SiO_2 and Si typically involves mixtures of Ar and O_2 with the addition of a fluorocarbon.[3,4] Recently, there has been a steadily growing interest in inductively coupled plasma (ICP) sources for numerous plasma-enhanced materials processing because the ICP sources provide stable, reproducible, and highly uniform high density plasmas. It has been known that most of O_2-Ar ICP discharges are characterized by high oxygen atom content.[5,6] O_2-Ar plasmas contain several important species, such as oxygen atoms, metastable oxygen molecules, ozone, and metastable and resonant state argon atoms.[7,8] In order to characterize the O_2-Ar ICP discharges, the important plasma parameters that characterize the discharge properties are the electron density, the electron temperature, and the electron energy distribution function (EEDF). Among these, the electron temperature is one of the most important plasma parameter because the change of electron temperature can influence the composition of radicals participating in the chemical reaction with the wafer. In addition, the number densities of various species in the plasma mentioned above are a significant concern. Global models have been developed to study the change of the concentrations of plasma species with the operating parameters.[9–11] However, since the chemistry in the model is too complex and the boundary condition at the reactor wall is hard to set up, it is somewhat inconvenient to apply the global model at industry environment. A considerable amount of plasma physics knowledge can be extracted from the plasma emission spectra. Optical emission spectroscopy (OES) is a non-intrusive technique that can monitor the change of the concentrations of the plasma species in real time.

Plasma emission from argon atom is used in many types of optical plasma diagnostics.[12–15] Especially, the electron temperature and the metastable densities can be estimated by several spectroscopic methods. One method is based on a simple collisional-radiative model utilizing the experimental relative emission intensities of only four argon lines that originate from any of the 4p argon levels.[16–18] Depending on the applications, the Ar content in the mixture can vary from less than a few percent (O_2-dominated discharge) to over 90% (Ar-dominated discharge). The gas pressure is also dependent on the application and the sizes of ICP chamber and rf antenna. In order to meet the demand of the process, the plasma properties should be clarified for different gas pressure, Ar content, and rf power, and be tailored for a specific applications.

This paper is devoted to the implementation of a simple emissive spectroscopy technique for diagnostics of metastable argon atom, electron density and temperature, and dissociation fraction of oxygen molecules in inductively coupled O_2-Ar discharges with varying operating parameters. The operating parameters, such as Ar content in the gas mixture, applied rf power, and total gas pressure, have been varied in an attempt to fully characterize plasma parameters and oxygen atom production. The electron temperature is obtained by analyzing the optical emission spectra from excited Ar atoms and then compared with the values given by the Langmuir probe at different powers (200–600 W) in the pressure range 1–40 mTorr.

[a]Electronic address: thchung@dau.ac.kr.

In plasma processing, actinometry is a frequently used and well-developed technique to estimate the density of neutrals (O in this work). The optical emission actinometry has only a limited use in plasmas in which the content of the actinometer gas (Ar in this work) is less than a few percent (e.g., 5% or less). As was seen in our previous work,[19] the use of actinometry can be extended to the region of a higher Ar content although it gives a relatively rough estimate of the neutral O density. This work investigates the change of neutral O density with the control parameters using optical emission actinometry, and some physical explanation is given with a discussion of the plasma properties, such as the electron density, the electron temperature, and the electron energy distribution function measured by a Langmuir probe.

II. EXPERIMENT

The plasma generation chamber consists of a stainless steel cylinder with a diameter 28 cm and a length of 30 cm. A 1.9 cm thick by 27 cm diameter tempered glass plate mounted on the one end separates the planar one-turn induction coil from the plasma. The induction coil is made of copper (with water-cooling) and connected to an L-type capacitive matching network and an rf power generator. The details of the apparatus are found in Ref. 20.

The plasma chamber is evacuated by a diffusion pump, backed by a rotary pump, giving a base pressure of 9×10^{-6} Torr. The operating gas pressure is controlled by adjusting the mass flow controller. The O_2 gas pressure is varied in the range of 2–40 mTorr. And a 13.56 MHz generator with a power output of 200–600 W drives rf current in a flat one-turn coil through the rf power generator and matching network. An rf-compensated cylindrical single Langmuir probe was mounted through one of the ports on the vacuum chamber. The probe tip made of tungsten with a diameter of 0.1 mm and a length of 10 mm is used to measure the plasma parameters. The probe tip was located on the axis of the cylinder at 14 cm below the tempered glass plate. Probe circuit resistance is accounted for by the use of the reference ring probe with a resonance filter that reduces the rf distortion of probe characteristics.[21]

To measure plasma parameters, the harmonic technique, which exploits the generation of harmonics resulting from excitation of the nonlinearity of the single Langmuir probe characteristics, combined with Druyvesteyn method was used.[22] In the harmonic method, the voltage applied to a probe consists of the sweep voltage and the sinusoidal voltage v_0 of the frequency ω. The second harmonic term $I_{2\omega}$ of the measured probe current is proportional to the second derivative as $I_{2\omega} \approx (1/4)\, v_0^2\, (d^2I/dV^2) \cos 2\omega t$, which is related to the electron EEDF, $f(\epsilon)$,

$$f(\epsilon) = \frac{2m}{e^2 S}\left(\frac{2\,\mathrm{eV}}{m}\right)^{1/2} \frac{d^2I}{dV^2}, \tag{1}$$

where e is the electron charge, S is the probe area, m is the mass of electron, V is the probe potential referenced to the plasma potential (V_p), and ϵ is measured in units of eV. The electron density (n_e) and the effective electron temperature (T_e) are calculated with the measured EEDF as follows:

$$n_e = \int_0^{\epsilon_{max}} f(\epsilon)d\epsilon, \quad T_e = \frac{2}{3n_e}\int_0^{\epsilon_{max}} \epsilon f(\epsilon)d\epsilon, \tag{2}$$

where ϵ_{max} is determined by the dynamic range of the EEDF measurement. The electron temperature can also be determined from the slope of the probe I-V curve in the exponential region (from the point where the probe current is zero to where the slope of the curve begins to decrease). We observed that both methods yield almost same values of the electron temperature.

Langmuir probes are very efficient at measuring the EEDF at low energies, but reliable measurements become more difficult at high energies.[21] This difficulty is due to a combination of lower signal size (orders of magnitude fewer electrons than at lower energies) and a non-negligible contribution to the recorded probe current from ions. In contrast, the OES signal arising from electron-impact excitation of ground state atoms is only sensitive to high energy electrons.[12]

In this work, the light intensity of emissive molecules and radicals in the plasma was focused by means of optical fiber into entrance slit of 0.75 m monochromator (SPEX 1702), equipped with a grating of 1200 grooves per millimeter and slit width of 100 μm. The light was collimated at the exit slit where a photomultiplier tube (Hamamatsu R928) converted photons into an electric signal. Optical emission spectra were recorded in the wavelength range of 250–850 nm with a resolution of 0.1 nm. The measured emission spectra were corrected for the spectral response of the detection system, which includes optical fiber, monochromator, and photomultiplier tube. The detection system was calibrated in intensity between 250 to 850 nm using a quartz halogen lamp with a known spectral radiance. The dependence of the emission intensities on the plasma parameters was investigated.

III. OPTICAL EMISSION SPECTROSCOPY

As mentioned above, the determination of plasma density and electron temperature is needed to optimize the plasma process for most of plasma applications. Optical emission spectroscopy provides a non-intrusive method for this purpose. The observed optical emission intensity for a selected transition from certain electron-excited states is given by

$$I(\nu_X) = K(\nu_X)\, h\nu_X A\, [X], \tag{3}$$

where h is the Planck's constant, ν_X is the frequency of the transition, [X] is the number density of species X, and A is the optical emission probability for the transition, $K(\nu_X)$ is the total optical detection efficiency at ν_X involving all of the steps from emission light collection, optical fiber transfer, and monochromator transportation up to the detector response.[23]

The emission lines from excited argon are the most abundant, and these have reliable transition probability values published in the literature. Assuming that upper levels of the selected atomic transitions are in local thermodynamic

equilibrium (LTE), we can use the conventional Boltzmann plot technique to determine the excitation temperature

$$\ln\left(\frac{I_{ij}}{K_{ij}A_{ij}g_i\nu_{ij}}\right) = -\frac{E_i}{k_B T_{exc}} + const, \tag{4}$$

where I_{ij}, ν_{ij}, K_{ij}, and A_{ij} are the intensity, the frequency, the detector efficiency, and the Einstein coefficient of the spectral line from $i \rightarrow j$ level, respectively, g_i is the degeneracy or statistical weight of the emitting upper level i of the studied transition, k_B is the Boltzmann constant, and E_i is the excitation energy of level i. This model assumes that electron collisions between excited atoms are dominant in populating and depopulating in excited atoms. Most of the plasmas deviate from LTE, especially for all types of low density plasma in laboratories. Deviations from LTE are due to the mass difference between electrons and positive ions, strong gradients in the plasma, and the associated diffusion effects. Since LTE can be verified for the high energy levels close to ionization threshold, low-temperature plasmas are partial LTE. Even in the case of local thermal equilibrium conditions, T_e can be very different from estimated T_{exc}, which gives us only information about low-energy region of electron energy distribution function.

In general, RF low-pressure plasmas have a small degree of ionization, which makes collisional processes less efficient than in plasmas with higher electron densities and, consequently, radiative processes become important. Especially, in inductively coupled low-pressure O_2-Ar plasmas, direct excitation from the ground state with radiative decay can be assumed to dominate over the production and the destruction of excited energy levels. For instance, many excited states of argon are mainly produced by electron-impact excitation from the ground state,[24] and the quenching rate of excited oxygen and argon atoms by both O_2 molecules and Ar atoms is very small compared to the radiative decay. This simplification is called the corona balance. Gordillo-Vázquez *et al.*[24] have investigated the corona model and obtained a modified Boltzmann formula as follows:

$$\ln\left(\frac{I_{ij}\Sigma_{j<i}A_{ij}}{K_{ij}A_{ij}a_{1i}\nu_{ij}}\right) = -\frac{E_i}{k_B T_{e\mathrm{OES}}} + const, \tag{5}$$

where a_{1i} is the coefficient in an exponential approximation of the electron impact excitation rate coefficient from ground state to level i. The inverse of the slope of the best linear fitting gives the electron temperature estimated by the corona model $T_{e\mathrm{OES}}$. However, when the electron density is so high that de-excitation by electron collisions dominates radiative decays, the corona model is not valid. Especially, because highly excited levels have long radiative lifetimes, an atom is likely to undergo an electron-atom collision before it has time to radiatively decay.[13] The main source of error for determining $T_{e\mathrm{OES}}$ is the use of inaccurate values of A_{ij} and a_{1i}. The errors become large for low-Ar content and for higher pressure discharges. Additionally, the strong emission lines in argon spectrum come essentially from the levels with close energy values.[25] The excitation temperature obtained by Eq. (4) gives a first estimate of the electron temperature in the low-pressure plasmas. In this study, a comparison is made between T_{exc} and $T_{e\mathrm{OES}}$ in argon and argon-oxygen plasmas generated with a wide variety of control parameters. As a reference, T_e obtained by Langmuir probe technique will also be compared.

The corona model can be extended to consider the optical transitions originating from the metastable states. In pure argon, metastable atoms provide a basic intermediate state for excitation and ionization. The apparent cross section, $\sigma_i^{App}(\epsilon)$, includes the effect of excitation into higher levels followed by radiative decay into level i. The optical emission cross section from i to j level can be defined as[13,26]

$$\sigma_{i\rightarrow j}^{Opt}(\epsilon) = \frac{A_{ij}\,\sigma_i^{App}(\epsilon)}{\Sigma_{l<i}A_{il}}. \tag{6}$$

Assuming a Maxwellian energy distribution for electrons, the observed light intensity incident on a detector for a particular $i \rightarrow j$ emission line is written as

$$I_{ij} = C_{ij}h\nu_{ij}\,n_e n_0\sqrt{\frac{2}{\pi}}T_e^{-3/2}\int_0^\infty \sigma_{i\rightarrow j}^{Opt}(\epsilon)\,\epsilon\, e^{-\epsilon/T_e}\,d\epsilon, \tag{7}$$

where n_0 is the neutral atom density and C_{ij} is the proportionality constant.

Consider the Ar peaks at 750.4 nm ($2p_1 \rightarrow 1s_2$), 794.8 nm ($2p_4 \rightarrow 1s_3$), and 811.5 nm ($2p_9 \rightarrow 1s_5$). These emission lines originate from the excitation from the ground state and from the metastable state. For the case of $2p_1$ level, the population processes are dominated by excitation from the ground state and $1s_3$ metastable level while the depopulation processes are represented by radiative decay to the $1s_2$ state (750.4 nm). Therefore, we have

$$I_{750} = C_{750}h\nu_{750}\,n_e\,T_e^{-3/2}\left[[\mathrm{Ar}]\int_0^\infty \sigma_{750,g}^{Opt}(\epsilon)\,\epsilon\, e^{-\epsilon/T_e}\,d\epsilon + [\mathrm{Ar}(1s_3)]\int_0^\infty \sigma_{750,m}^{Opt}(\epsilon)\,\epsilon\, e^{-\epsilon/T_e}\,d\epsilon\right], \tag{8}$$

where $\sigma_{750,g}^{Opt}(\epsilon)$ and $\sigma_{750,m}^{Opt}(\epsilon)$ are measured optical emission cross sections from the ground state to $2p_1$ and from the metastable $1s_3$ to $2p_1$.

Similarly, for the case of $2p_9$ level, the population processes are dominated by excitation from the ground state and $1s_5$ metastable level while the depopulation processes are represented by radiative decay to the $1s_5$ state (811.5 nm),[12,13] then we have

$$I_{811} = C_{811}h\nu_{811}\,n_e\,T_e^{-3/2}\left[[\mathrm{Ar}]\int_0^\infty \sigma_{811,g}^{Opt}(\epsilon)\,\epsilon\, e^{-\epsilon/T_e}\,d\epsilon + [\mathrm{Ar}(1s_5)]\int_0^\infty \sigma_{811,m}^{Opt}(\epsilon)\,\epsilon\, e^{-\epsilon/T_e}\,d\epsilon\right], \tag{9}$$

where $\sigma_{811,g}^{Opt}(\epsilon)$ and $\sigma_{811,m}^{Opt}(\epsilon)$ are measured optical emission cross sections from the ground state to $2p_9$ and from the metastable $1s_5$ to $2p_9$.

For the case of $2p_4$ level, the population processes are dominated by excitation from the ground state and $1s_3$

metastable level while the depopulation processes are represented by radiative decay to the 4 s state such as 794.8 nm ($2p_4 \rightarrow 1s_3$) and 852.1 nm ($2p_4 \rightarrow 1s_2$).[12,18] Therefore,

$$I_{794} = C_{794} h\nu_{794}\, n_e\, T_e^{-3/2} \left[[\mathrm{Ar}] \int_0^\infty \sigma^{Opt}_{794,g}(\epsilon)\, \epsilon\, e^{-\epsilon/T_e}\, d\epsilon + [\mathrm{Ar}(1s_3)] \int_0^\infty \sigma^{Opt}_{794,m}(\epsilon)\, \epsilon\, e^{-\epsilon/T_e}\, d\epsilon \right], \quad (10)$$

while $\sigma^{Opt}_{794,g}(\epsilon)$ and $\sigma^{Opt}_{794,m}(\epsilon)$ are measured optical emission cross sections from the ground state to $2p_4$ and from the metastable $1s_3$ to $2p_4$.

The experimentally obtained values of I_{811}/I_{750} and I_{794}/I_{750} with a pre-determined T_e using Eq. (2) or (5) allow us to estimate the metastable argon densities $[\mathrm{Ar}(1s_3)](=n_{1s_3})$ and $[\mathrm{Ar}(1s_5)](=n_{1s_5})$ by utilizing the cross section data in the literature.[27,28] If direct measurements of the metastable number densities can be made by other means, a measured value of I_{811}/I_{750} or I_{794}/I_{750} results in the determination of T_e. Although the addition of oxygen changes the excited state kinetics of argon,[4] this method can also be applied to O_2-Ar plasmas with a large Ar content.

Another important parameter for oxygen-containing plasmas is the oxygen atom density in the plasma. A comparison of the intensity of 844 nm line from oxygen atom with that of the argon 750 nm line can give an estimation of the dissociation fraction. The population dynamics of the upper atomic oxygen state ($O(3p\,^3P)$) of 844.6 nm transition is governed by direct electron impact excitation and dissociative excitation from the ground state O atom, radiation losses, and collision-induced quenching. In low-temperature oxygen plasmas, the main neutral constituent is O_2. Therefore, the dissociative excitation process must be also considered since it often yields a very important contribution. Then, the balance equation of oxygen atom is written as

$$n_e(k_e^{3P}[\mathrm{O}] + k_{de}^{3P}[\mathrm{O_2}]) = (\Sigma A_{ij}^{3P} + k_Q^{3P}[\mathrm{O_2}])[\mathrm{O}(3p\,^3P)], \quad (11)$$

where k_Q^{3P} is the quenching rate coefficient of $O(3p\,^3P)$ in O_2, k_e^{3P} the rate coefficient for electron-impact direct excitation to $O(3p\,^3P)$ from the ground-state O, k_{de}^{3P} the rate coefficient for electron-impact dissociative excitation to $O(3p^3\,^3P)$ from the ground-state O_2, and ΣA_{ij}^{3P} is the sum of Einstein probability from $O(3p\,^3P)$. Since the majority of the atom density is in the ground electronic state, the balance equation can give the atomic O density.[29] Using actinometry, the dissociation fraction of O_2 can be calculated as[30]

$$\frac{[\mathrm{O}]}{[\mathrm{O_2}]} = \frac{K_{750}}{K_{844}} \frac{\nu_{750}}{\nu_{844}} \frac{A_{750}}{A_{844}} \frac{k_{Ar}^{dir}}{k_e^{3P}} \frac{(\Sigma A_{ij}^{3P} + k_Q^{3P}[\mathrm{O_2}])}{(\Sigma A_{ij}^{2p_1} + k_Q^{2p_1}[\mathrm{O_2}])} \frac{[\mathrm{Ar}]}{[\mathrm{O_2}]} \frac{I_{844}}{I_{750}} - \frac{k_{de}^{3P}}{k_e^{3P}}, \quad (12)$$

where $k_Q^{2p_1}$ is the quenching rate coefficient of excited $Ar(2p_1)$ in O_2, and k_{Ar}^{dir} is the rate coefficient for electronic excitation to $2p_1$ of the ground state Ar.

IV. RESULTS AND DISCUSSION

Figure 1(a) presents a typical optical emission spectrum of an ICP Ar plasma operated at the pressure of 10 mTorr and the power 500 W. Within the range of the wavelength considered in this work, the emission lines can be categorized into several groups: the Ar $2p \rightarrow 1s$ transition (660–1150 nm), the Ar $3p \rightarrow 1s$ transition (410–480 nm), the Ar ion transition (300–500 nm), and the other lines. The Ar $3p \rightarrow 1s$ transition lines are shown at 415.9 nm ($3p_6 \rightarrow 1s_5$), 418.2 nm ($3p_2 \rightarrow 1s_3$), 419.8 nm ($3p_5 \rightarrow 1s_4$), 420.1 nm ($3p_9 \rightarrow 1s_5$), 425.9 nm ($3p_1 \rightarrow 1s_2$), 427.7 nm ($3p_7 \rightarrow 1s_4$), 430.0 nm ($3p_8 \rightarrow 1s_4$), 433.4 nm ($3p_3 \rightarrow 1s_2$), 451.8 nm ($3p_5 \rightarrow 1s_2$), and 470.2 nm ($3p_{10} \rightarrow 1s_2$).

There exist many Ar peaks associated with the $2p \rightarrow 1s$ transitions at 750.4 nm ($2p_1 \rightarrow 1s_2$), 811.5 nm ($2p_9 \rightarrow 1s_5$), 696.5 nm ($2p_2 \rightarrow 1s_5$), 706.7 nm ($2p_3 \rightarrow 1s_5$), 738.3 nm ($2p_3 \rightarrow 1s_4$), 763.5 nm ($2p_6 \rightarrow 1s_5$), 772.4 nm ($2p_2 \rightarrow 1s_3$), 794.8 nm ($2p_4 \rightarrow 1s_3$), 810.4 nm ($2p_7 \rightarrow 1s_4$), and 801.4 nm ($2p_8 \rightarrow 1s_5$). The emission lines from Ar ion are shown at 358.8 nm ($4p\,^4F \rightarrow 4s\,^4D$) and 434.8 nm ($4p\,^4D \rightarrow 4s\,^4P$). In addition to the lines mentioned above, the lines at 383.5 nm ($4p \rightarrow 1s$), 394.9 nm ($3p \rightarrow 1s$), 518.7 nm ($5s \rightarrow 2p$), 549.6 nm ($6d \rightarrow 2p$), 555.9 nm ($5d \rightarrow 2p$), 559.7 nm ($6s \rightarrow 3p$), 588.3 nm ($3s \rightarrow 2p$), 603.2 nm ($5d \rightarrow 2p$), 641.3 nm ($3s \rightarrow 2p$), and 657.3 nm ($5d \rightarrow 2p$) are also observed. In the argon discharge, the highest emission intensities have been recorded in the wavelength range of 750–850 nm.

The intensity peaks from the Ar $3p \rightarrow 1s$ transitions are suppressed as the pressure is increased (even though the amount of Ar atoms is increased). This may result from that T_e is decreased with increasing pressure. The 750.4 nm Ar emission intensity is proportionally increased with increasing power, which indicates that the increased electron density is responsible for an increase in the excitation rate of Ar atoms to the $2p_1$ state. The emission intensities of the transition Ar $3p \rightarrow 1s$ are also increased with power in an almost similar fashion. The 358.8 nm, 434.8 nm, and 479.8 nm emission intensities provide a reasonable estimate of the relative concentration of Ar ions. The primary effect of increasing power is to increase the fraction ionization of the gas, while only modestly affecting the electron temperature.[31] Although the emission intensities from argon ion increases with power, the intensity ratios of these lines to the 750.4 nm line decrease slightly with power. These ratios also decrease with increasing pressure and Ar content. This observation indicates that the increase of excitation of Ar atoms becomes larger than that of Ar ions with increasing pressure and Ar content.

Figure 1(b) presents a typical optical emission spectrum of an ICP O_2 plasma operated at the pressure of 10 mTorr and the power 500 W. Many peaks associated with optical transitions of O atom are observed: 436.8 nm from ($O(4p\,^3P \rightarrow 3s\,^3S)$), 777.4 nm ($O(3p\,^5P \rightarrow 3s\,^5S)$), 394.7 ($O(4p\,^5P \rightarrow 3s\,^5S)$), 645.4 nm ($O(5s\,^5S \rightarrow 3p\,^5P)$), 844.6 nm ($O(3p\,^3P \rightarrow 3s\,^3S)$), 700.2 nm ($O(4d\,^3D \rightarrow 3p\,^5P)$), 533.0 nm ($O(5d\,^5D \rightarrow 3p\,^5P)$), 595.8 nm ($O(5d\,^3D \rightarrow 3p\,^3P)$), and 725.4 nm ($O(5s\,^3S \rightarrow 3p\,^3P)$). The highest intensity corresponds to the 777.4 nm line. There were emission bands in the wavelength range of 520–530 nm and 550–565 nm from O_2^+ ($b\,^4\Sigma_g^- \rightarrow a\,^4\Pi_u$), but no evidence of strong O_2 emission was found. The intensities of the O peak and O_2^+ bands were found to decrease with increasing pressure.

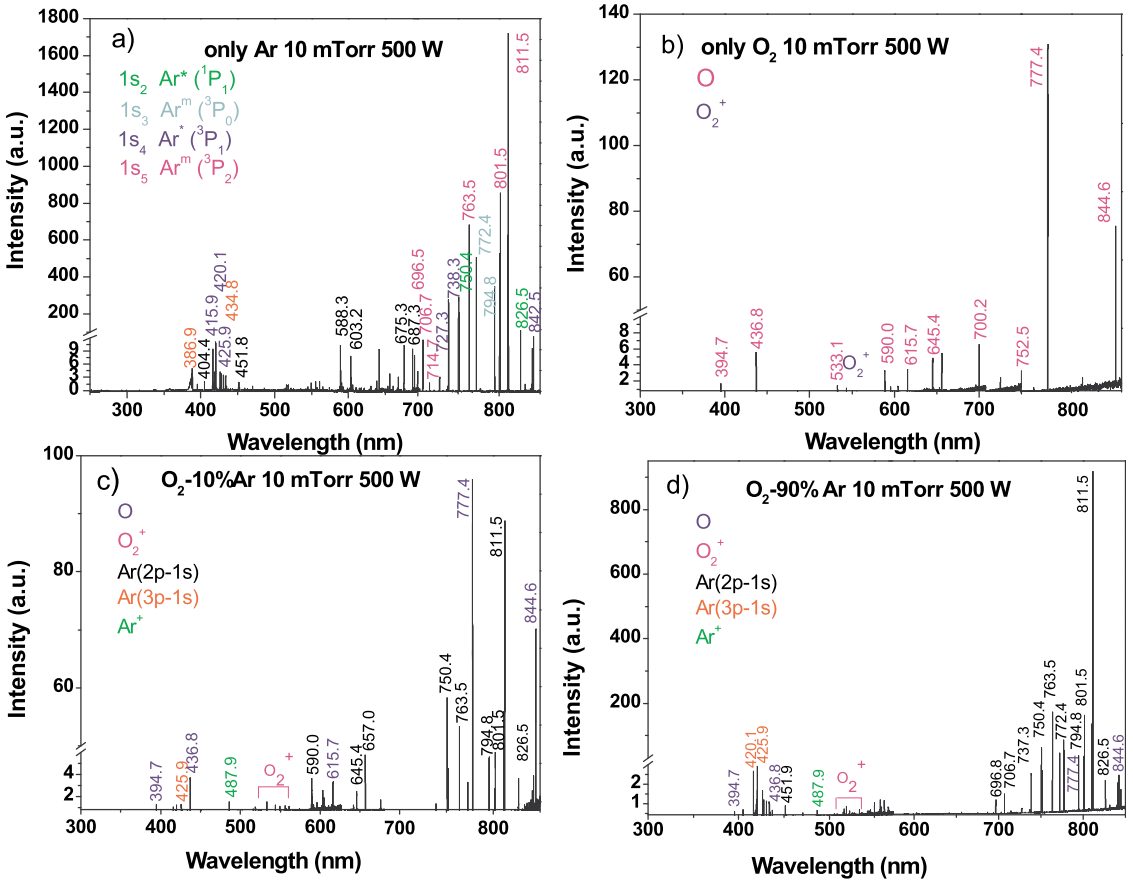

FIG. 1. Spectra of optical emission from inductively coupled (a) Ar discharge at $p = 10$ mTorr and $P = 500$ W (the distinct color lettering of the peaks denotes the corresponding lower level of the optical transitions), (b) O_2 discharge at $p = 10$ mTorr and $P = 500$ W, (c) O_2-10%Ar discharge at $p = 10$ mTorr and $P = 500$ W, and (d) O_2-90%Ar discharge at $p = 10$ mTorr and $P = 500$ W. For (b)-(d), the distinct color lettering of the peaks or the bands denotes the categories of the optical transitions from specific species.

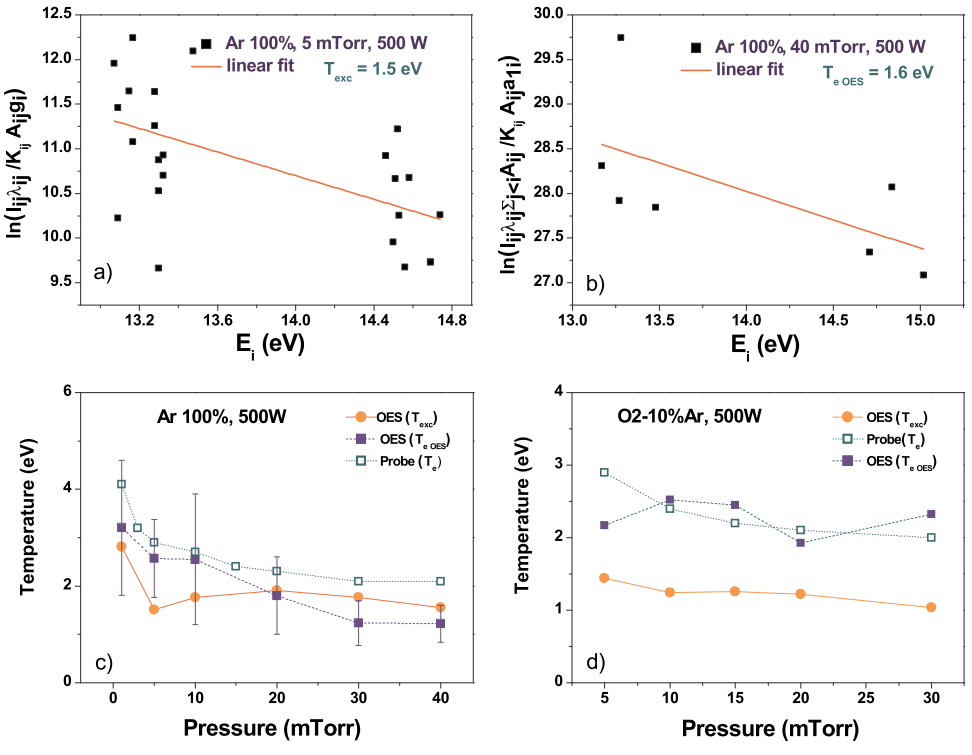

FIG. 2. (a) The conventional and (b) modified Boltzmann plots obtained from Ar lines for 1.5 mTorr and (b) 40 mTorr of the O_2-100%Ar plasma at 500 W. T_{exc} and T_{eOES} values deduced from linear fit are indicated. E_i is the energy of the upper levels of the radiative transition. The electron temperatures measured by OES and by the Langmuir probe are compared as a function of pressure for (c) pure Ar discharge and (d) O_2-10%Ar discharge. The pressure range is from 1.0 mTorr to 40 mTorr and $P = 500$ W (All axes suppress zero point).

Figures 1(c) and 1(d) present typical optical emission spectra of ICP O_2-Ar plasmas operated in different Ar contents (10% and 90%). The main emission peaks correspond to several transition lines of atomic oxygen and argon and of molecular oxygen. The emission intensities of all peaks significantly increased with power, while they overall decreased with pressure, presumably due to a decrease in T_e. But the normalized intensities of 844 nm and 777 nm lines to the 750 Ar line was observed to increase slightly with pressure (data not shown). The Ar content in the gas mixture does not make a noticeable influence on the emission intensities of the typical lines of O. By decreasing the amount of molecular O_2 with increasing Ar content, the number densities of excited atomic O and O_2^+ would also decrease. However, with the addition of Ar, Penning excitation and Penning dissociation due to Ar^m cause the densities of the excited states of O, O_2, and O_2^+ to increase trading off the decrease in the amount of O_2. An increase in the Ar content results in a slight increase of the emission intensity from O atoms. As the Ar content is increased, the line intensities from Ar atoms and Ar ions including O atoms increase in a nearly linear manner, indicating an enhancement in excitation frequency, presumably because of an increased number density of higher energy electrons. Especially, at 70% Ar content, the 811 nm line intensity shows a drastic increase, which may be caused by the increase in Ar metastable. The normalized line intensities from the argon ions at 358.8 nm and 434.8 nm lines to the 750 Ar line is observed to decrease with Ar content (data not shown). This ratio of intensity is also observed to slightly decrease with increasing pressure and power while the ratio of the emission intensity of $3p \rightarrow 1s$ to that of $2p \rightarrow 1s$ remains unchanged with pressure and power.

We can proceed to evaluate the excitation temperature and the electron temperature in our plasmas by using the conventional (Eq. (4)) and the modified Boltzmann plot method (Eq. (5)). We present in Figs. 2(a) and 2(b) the conventional and modified Boltzmann plots corresponding to pure Ar plasmas. The error bar includes the uncertainty associated with the spectral response of the detection system and the error due to the dispersion exhibited by the experimental data. Figure 2(c) shows the changes of $T_{e\mathrm{OES}}$ and T_{exc} as a function of pressure in pure argon discharges. The conventional Boltzmann plot is found to have a little larger slopes than those of the modified Boltzmann plot. Therefore, T_{exc} is a little less than $T_{e\mathrm{OES}}$. This may be connected to the fact that T_{eOES} derived from the coronal model is sensitive to the high energy tail of the electron energy distribution function since it only assumes ground state excitation. The observation that T_{exc} is less than $T_{e\mathrm{OES}}$ is in contrary to the case of the capactive discharges operating at the pressures of several hundreds mTorr.[24] However, both the plots give a reasonable estimate of average energy of electrons, and the variation trends of $T_{e\mathrm{OES}}$ and T_{exc} with operating parameters are observed to be similar. As we will see later, the Langmuir probe method provides values of T_e comparable to $T_{e\mathrm{OES}}$. This can be explained by the fact that the T_e obtained by the EEDF integration method (Eq. (2)) accounts for the contribution from all the energy range of electrons. For plasmas with low Ar content (Fig. 2(d)), the difference between $T_{e\mathrm{OES}}$ and T_e from the probe method is observed to be a little larger compared to that in the pure argon discharge.

But the difference between $T_{e\mathrm{OES}}$ and T_{exc} is observed to depend on the operating parameters. Figure 3 shows the changes of $T_{e\mathrm{OES}}$ and T_{exc} as functions of power and Ar content. When the gas pressure goes to 40 mTorr, the difference becomes small. This can be explained by a depletion of the electron population in the high-energy region with the pressure increase. In a general statement, the electron temperature decreases with increasing pressure, power, and Ar content. The difference between $T_{e\mathrm{OES}}$ and T_e measured by a Langmuir probe is observed to be not significant.

The calculated density ratios n_{1s_5}/n_g and n_{1s_3}/n_g are shown in Fig. 4 (n_g is the ground state density of Ar atoms).

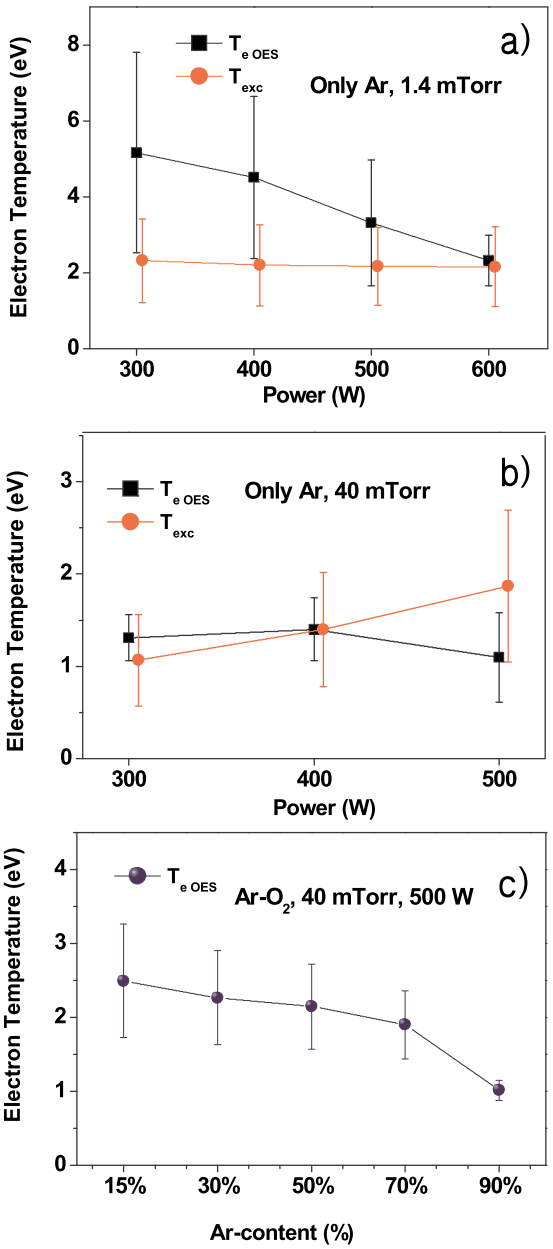

FIG. 3. Comparison of the electron temperatures and the excitation temperatures measured by the OES models as a function of power for (a) pure Ar discharges at 1.4 mTorr and (b) at 40 mTorr. (c) The electron temperatures as a function of the Ar content at 40 mTorr O_2-Ar discharge.

In pure argon discharges, the ratio n_{1s_5}/n_g decreases with increasing pressure whereas the ratio n_{1s_3}/n_g increases slightly. In O_2-10% Ar discharges, the ratio n_{1s_5}/n_g becomes about three times lower compared to that in pure Ar discharges. This is connected to the fact that the quenching of metastables by oxygen will begin to dominate at higher oxygen abundances, and thereby the discharge will resemble more and more discharges in pure oxygen.[4] This phenomenon has some implications in estimating the dissociation fraction of oxygen molecules for O_2-Ar discharges. More elaborate OES model should take into account cascading contributions from higher excited states, collisional excitation from metastable states, and also from photon reabsorption.[14]

As we will see later in Eq. (13), in order to accurately estimate the dissociation fraction of oxygen molecules in Ar-O_2 plasmas, it is necessary to determine not only the electron temperature but also the electron density. Figures 5(a) and 5(b) show the evolutions of the electron density and the electron temperature obtained by the electric probe with pressure in Ar and O_2 plasmas. As expected, in Ar plasmas, the electron density increases with increasing pressure while the electron temperature decreases with it. In pure O_2 plasmas, the electron density is lower than that of Ar plasmas since the electrons lose their energy via various loss channels such as ionization and excitation, including vibration and rotation collisions, as well as the escape to the chamber walls. However, both Ar and O_2 plasmas are observed to have comparable electron temperature. In addition, it is

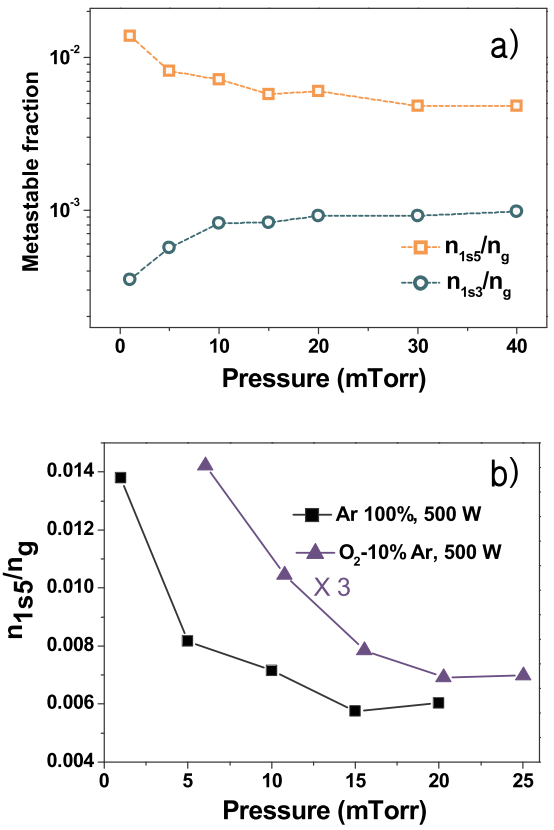

FIG. 4. Calculated fractions of metastable argon atoms (n_{1s_5}/n_g and n_{1s_3}/n_g) in (a) pure Ar discharge and (b) a comparison of n_{1s_5}/n_g in pure Ar discharge with that (multiplied three times) in O_2-10%Ar discharge.

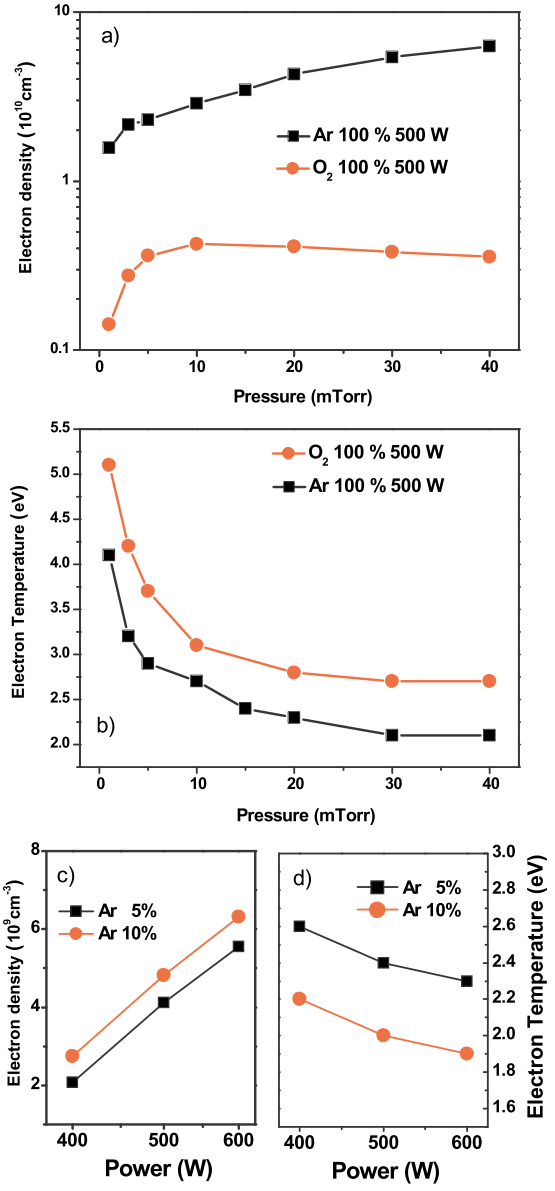

FIG. 5. Electric probe measurements; (a) electron densities (n_e) and (b) electron temperatures (T_e) as a function of pressure in Ar and O_2 discharges, and (c) n_e and (d) T_e as a function of power for two different Ar contents (5% and 10%) in 10 mTorr O_2-Ar discharges.

observed that n_e varies weakly with pressure compared to pure Ar plasmas over the range studied.[5] The electron density is observed to increase with increasing pressure at a low-pressure range, and have a maximum, and then decrease slightly. This behavior was also observed in our earlier works.[32,33]

Figures 5(c) and 5(d) present the electron density and the electron temperature as a function of power for two different Ar contents (5% and 10%) in 10 mTorr O_2-Ar plasmas. As expected, the electron density increases with increasing power while the electron temperature decreases slightly. With an increase in the Ar content, the electron density is observed to increase and the electron temperature decreases. This is due to the fact that there exist additional electron energy loss channels with O_2 addition. It should be noted that although not shown in the figure, the measured

EEDF can be considered as a Maxwellian distribution. This allows us to use Maxwellian electron energy distribution functions in obtaining the electron-impact rate coefficients (as in Eqs. (8)–(10)).

In oxygen plasmas, atomic oxygen species are mainly produced by the electron-impact processes such as dissociative collisions between electrons and oxygen molecules or between electrons and oxygen molecular ions (dissociative recombination). These processes depend strongly on the electron temperature. However, in oxygen-argon plasmas, there exists dissociation mechanism associated with the excited state Ar. Based on the actinometry, the dissociation fraction of oxygen molecules is calculated as functions of pressure and power as shown in Figs. 6(a) and 6(b). For O_2-Ar 5% discharge at 30 mTorr, the dissociation fraction is increased slightly from 0.028 to 0.031 with increasing power from 300 to 500 W. For O_2-Ar 10% discharge at 500 W, the dissociation fraction is increased slightly from 0.043 to 0.057 with increasing pressure. It should be noted that an enhancement of oxygen atom density is associated with an enhancement in the electron density (with higher energy), but a decrease in T_e is not necessarily associated with a decrease in dissociation fraction.[34] From global balance of the discharge kinetics, the dissociated neutral atom density is expected to be proportional to the power.[35] This is also confirmed in the figure.

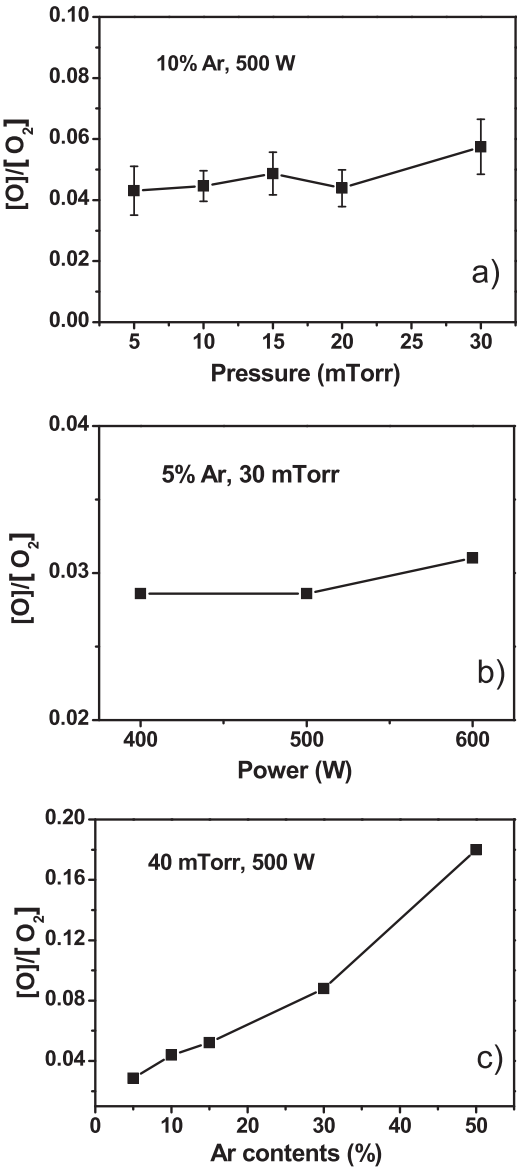

FIG. 6. Estimated dissociation fractions; (a) as a function of pressure at $p = 500$ W (with the Ar content 10%), (b) as a function of power at $p = 30$ mTorr (with the Ar content 5%), and (c) as a function of the Ar content at $p = 40$ mTorr and $P = 500$ W.

As shown in Fig. 6(c), the dissociation fraction is found to increase with increasing Ar content. The actinometry for larger Ar-content discharges would give an overestimated value for dissociation fraction because the Penning excitation of oxygen atoms due to excited Ar and/or dissociative excitation of oxygen molecules due to Ar metastables should be considered. The dissociation fraction considering the latter effect can be modified as

$$\left(\frac{[O]}{[O_2]}\right)_{\text{corrected}} = \frac{[O]}{[O_2]} - \frac{[Ar^m]k^m_{diss}}{n_e k^{3P}_e}, \tag{13}$$

where k^m_{diss} is the rate coefficient for Penning dissociation of oxygen molecule due to Ar metastable atoms.[10,36] Actually, because Penning dissociation process results in ground state and metastable oxygen atom, not excited oxygen atoms in the model process, the real rate coefficient in the correction term may be much less than k^m_{diss}. Although $[Ar^m]$ can be almost comparable to n_e in pure Ar plasmas (as was noticed from Fig. 4), normally $[Ar^m]$ is less than n_e in O_2-Ar plasmas, and k^{3P}_e is larger than k^m_{diss},[30] therefore the correction term is not significant, and Eqs. (12) and (13) could be utilized to calculate the dissociation fraction for oxygen discharges with a higher Ar content under the operating conditions of this study. The value of $[Ar^m]$ can also be determined with advanced diagnostics methods such as laser induced fluorescence or laser absorption spectroscopy.[4] Then, the oxygen atom density can alternatively be calculated. The trend of change in the dissociation fraction correlates well with the electron density and the electron temperature presented in Fig. 5.

V. CONCLUSION

Optical emission spectroscopy of low-pressure inductively coupled argon, oxygen, and Ar-O_2 mixture plasmas was performed. It was found that although the emission intensities from argon ion increased with increasing power, the intensity ratios of these lines to the 750.4 nm line decreased slightly with power. These ratios also decreased with increasing pressure and Ar content. This observation indicates that the increase in excitation of Ar atoms becomes larger than that of Ar ions with increasing pressure and Ar content. By using the conventional and the modified Boltzmann plot methods, the excitation temperature (T_{exc}) and the electron temperature ($T_{e\text{OES}}$) were evaluated, respectively, and the change of these temperatures was explored as functions of pressure, Ar content, and power. The T_{exc}, derived from the conventional (LTE) Boltzmann plot, was a little less than $T_{e\text{OES}}$ derived from the corona model. This is connected to the fact that $T_{e\text{OES}}$ is sensitive to the high energy

tail of the electron energy distribution function since it only assumes ground state excitation. Although T_{exc} is found to be a little less than $T_{e\mathrm{OES}}$, both give a reasonable estimate of electron temperature and have a similar behavior of change with operating parameters. When the gas pressure goes to 40 mTorr, the difference between T_{exc} and $T_{e\mathrm{OES}}$ even becomes small. It was also found that, in general, T_e decreased with increasing pressure and slightly decreased with increasing Ar content and power. Generally, the Langmuir probe method provided values of T_e comparable to those from the OES model. In Ar-O_2 discharges, the dissociation fraction of O_2 increases with increasing power and Ar content. The actinometry method to obtain the dissociation fraction employed in this work could also be applied to Ar-O_2 mixture plasmas with a large Ar content.

ACKNOWLEDGMENTS

This work was supported by the National Research Foundation of Korea (NRF) funded by the Ministry of Education, Science, and Technology (Grant No 20110018735, Fusion Core Research Center Program).

[1]D. L. Flamm, Plasma Chem. Plasma Process. **1**, 37 (1981).
[2]A. Granier, F. Nicolazo, C. Vall'ee, A. Goullet, G. Turban, and B. Grolleau, Plasma Sources Sci. Technol. **6**, 147 (1997).
[3]T. Sato and T. Makabe, J. Appl. Phys. **98**, 113304 (2005).
[4]Y. Hayashi, S. Hirao, Y. Zhang, T. Gans, D. O'Connell, Z. Lj. Petrovic, and T. Makabe, J. Phys. D: Appl. Phys. **42**, 145206 (2009).
[5]C. C. Hsu, M. A. Nierode, J. W. Coburn, and D. B. Graves, J. Phys. D: Appl. Phys. **39**, 3272 (2006).
[6]T. Sato and T. Makabe, J. Phys. D: Appl. Phys. **41**, 035211 (2008).
[7]K. Kutasi, V. Guerra, and P. A. Sa, Plasma Sources Sci. Technol. **20**, 035006 (2011).
[8]K. Kutasi, V. Guerra, and P. A. Sa, J. Phys. D: Appl. Phys. **43**, 175201 (2010).
[9]J. T. Gudmundsson, T. Kimura, and M. A. Lieberman, Plasma Sources Sci. Technol. **8**, 22 (1999).
[10]J. T. Gudmundsson and E. G. Thorsteinsson, Plasma Sources Sci. Technol. **16**, 399 (2007).
[11]E. G. Thorsteinsson and J. T. Gudmundsson, Plasma Sources Sci. Technol. **18**, 045001 (2009).
[12]J. B. Boffard, R. O. Jung, C. C. Lin, and A. E. Wendt, Plasma Sources Sci. Technol. **18**, 035017 (2009).
[13]J. B. Boffard, C. C. Lin, and C. A. DeJoseph, Jr., J. Phys. D: Appl. Phys. **37**, R143 (2004).
[14]M. Schulze, A. Yanguas-Gil, A. v. Keudell, and P. Awakowicz, J. Phys. D: Appl. Phys. **41**, 065206 (2008).
[15]N. Kang, S.-G. Oh, and A. Recard, J. Phys. D: Appl. Phys. **41**, 155203 (2008).
[16]D. Mariotti, Y. Shimizu, T. Sasaki, and N. Koshizaki, Appl. Phys. Lett. **89**, 201502 (2006).
[17]Y. K. Lee, K. T. Hwang, M. H. Lee, and C. W. Chung, J. Korean Phys. Soc. **52**, 1792 (2008).
[18]Y. K. Lee and C. W. Chung, J. Appl. Phys. **109**, 013306 (2011).
[19]T. H. Chung, Y. W. Lee, H. M. Joh, and M. A. Song, AIP Adv. **1**, 032136 (2011).
[20]M. A. Song, Y. W. Lee, and T. H. Chung, Phys. Plasmas **18**, 023504 (2011).
[21]V. A. Godyak, R. B. Piejak, and B. A. Alexandrovich, Plasma Sources Sci. Technol. **1**, 36 (1992).
[22]J. Y. Bang, A. Kim, and C. W. Chung, Phys. Plasmas **17**, 064502 (2010).
[23]Z. Liu, S. Li, Q. Chen, L. Yang, and Z. Wang, Plasma Sci. Technol. **13**, 458 (2011).
[24]F. J. Gordillo-Vázquez, M. Camero, and C. Gómez-Aleixandre, Plasma Sources Sci. Technol. **15**, 42 (2006).
[25]C. Foissac, C. Dupret, and P. Supiot, J. Phys. D: Appl. Phys. **42**, 015206 (2009).
[26]J. B. Boffard, B. Chiaro, T. Weber, and C. C. Lin, At. Data Nucl. Data Tables **93**, 831 (2007).
[27]H. A. Hyman, Phys. Rev. A **18**, 441 (1978).
[28]A. Dasgupta, M. Blaha, and J. L. Giuliani, Phys. Rev. A **61**, 012703 (1999).
[29]M. Gupta, T. Owano, D. Baer, and A. OKeefe, Appl. Phys. Lett. **89**, 241503 (2006).
[30]D. Pagnon, J. Amorim, J. Nahorny, M. Touzeau, and M. Vialle, J. Phys. D: Appl. Phys. **28**, 1856 (1995).
[31]J. S. Mckillop, J. C. Forster, and W. M. Holber, J. Vac. Sci. Technol. A **7**, 908 (1989).
[32]D. C. Seo, T. H. Chung, H. J. Yoon, and G. H. Kim, J. Appl. Phys. **89**, 4218 (2001).
[33]D. C. Seo and T. H. Chung, J. Phys. D: Appl. Phys. **34**, 2854 (2001).
[34]N. Itagaki, S. Iwata, K. Muta, A. Yonesu, S. Kawakami, N. Ishii, and Y. Kawai, Thin Solid Films **435**, 259 (2003).
[35]M. A. Lieberman and A. J. Lichtenberg, *Principles of Plasma Discharge and Materials Processing* (Wiley, New York, 1994), p. 487.
[36]K. Takechi and M. A. Lieberman, J. Appl. Phys. **90**, 3205 (2001).